# Biophysical model for gamma rhythms in the olfactory bulb via subthreshold oscillations

Jorge N. Brea[a,1], Leslie M. Kay[b,c], and Nancy J. Kopell[a,b,d,1]

[a]Center for BioDynamics and [d]Department of Mathematics and Statistics, Boston University, Boston, MA 02215; and [b]Institute for Mind and Biology and [c]Department of Psychology, University of Chicago, Chicago, IL 60637

Contributed by Nancy J. Kopell, October 23, 2009 (sent for review August 8, 2009)

**Gamma oscillations in the olfactory bulb can be produced as an interaction of subthreshold oscillations (STOs) in the mitral cells (MCs) with inhibitory granule cells (GCs). The mechanism does not require that the GCs spike, and we work in a regime in which the MCs fire at rates lower than the fast gamma rhythm they create. The frequency of the network is that of the STOs, allowing the gamma to be modulated in amplitude with only small changes in frequency. Gamma oscillations could also be obtained with spiking GCs, but only for GCs firing close to population rate. Our mechanism differs from the more standard description of the gamma oscillation, in which the the decay time of the inhibitory cells is critical to the frequency of the network.**

mitral cell | granule cell | graded inhibition

Gamma oscillations (40–100 Hz) are produced in the mammalian olfactory bulb (OB) and many other structures in the nervous system (1–3). In the neocortex and the hippocampus, gamma oscillations are believed to depend on fast-spiking interneurons, created either by the interaction of inhibitory cells alone or as an interaction of excitatory pyramidal cells and inhibitory interneurons, such as basket cells (4, 5). It is generally accepted that interactions between excitatory mitral cells (MCs) and inhibitory granule cells (GCs) at the dendrodendritic reciprocal synapse support gamma oscillations in the OB, but the physiological mechanisms of these oscillations are not well understood. Many slice studies focus on regimes in which the axonless GCs spike. However, it has been suggested, by contrast, that gamma oscillations in the OB depend on the subtheshold oscillations (STOs) in MCs, the excitatory cells of the OB (6), and that spikes from the GCs, the inhibitory cells of the OB, may not play a major part in the gamma oscillation of the OB (ref. 7 and see also *Discussion*). It is not understood what differences these features might make in the mechanism of synchronization of the OB gamma rhythm.

It is well known that a target population of cells can be synchronized by a common pulse of inhibition (5, 8, 9). The synchronization comes mainly from a shared suppression of firing until the inhibition has worn off sufficiently for the excitatory cells to fire. If the target cells are identical in drive, they will fire simultaneously; if they have somewhat different drives, they will fire with a small lag (5). With graded inhibition, it is less clear how the inhibition provides the synchronization: there is no clear decay time of inhibition, because the amplitude and time course of the inhibition is not stereotyped.

Here, we show that the features of STOs and graded inhibition can work together to produce a mechanism for the synchronization of gamma. We are interested in the regime in which MCs, the excitatory cells of the OB, spike with a firing rate significantly below that of the population frequency, as seen experimentally (10). Unlike the classical excitation–inhibition of the pyramidal interneuron network gamma (PING), in which the decay time of $GABA_A$-mediated inhibition is the most important time constant, STOs provide another time constant; in our hands, that is the most important mechanism for determining the population rhythm. The graded inhibition acts to synchronize the STOs and does not synchronize the spikes of the MCs, which are roughly locked to particular phases of the STOs and do not occur on every STO cycle. The graded inhibition is determined by the activity of the population MC spiking, which feeds back inhibition at times related to the STO activity. We show that autonomous periodic forcing of the STOs can act like this feedback, even for MCs that are deprived of spiking currents. Forcing by Gaussian noise does not synchronize STOs with different frequencies, nor does forcing by Poisson noise with a related rate. When there are STOs, spiking GC dendrites (GCDs) can also synchronize the population by synchronizing the STOs without synchronizing the MC spikes. However, in our hands, this occurs only if the GCDs are driven strongly enough to spike at rates approaching that of the population frequency.

## Results

**MC Population Can Be Synchronized by Some Kinds of Common Inhibition.** To understand how graded inhibition can produce synchronization, we first deal with a population that has 100 MCs but only one GC, so the MCs get common input. In this work we distinguish graded inhibition from spiking inhibition by two main properties. First, as sketched in Fig. 1*A*, the activation of graded synapses (−66 mV in our model) occurs below the spiking threshold. Second, whereas the dynamics of the spiking inhibition depends only on its decay time and the all-or-none threshold, graded inhibition has a soft threshold where the synapse can be partially activated when close to its threshold value; in our model, partial activation is in the range of −66.5 to −65.5 mV (see *SI Appendix* for graded and spiking synapse equations). The input to the MCs increased substantially and rapidly at 300 ms from its minimum to its maximum in ≈50 ms. Fig. 1*B* contains a raster plot of the MCs when there is no connection to the GCD. In this simulation, the input to the MCs had noise and heterogeneous drive as described in *Methods*. Without the connection to the GCD, the natural period of the MC STOs varied between 64 and 72 Hz.

Fig. 1*C Left* contains the raster plot of the population of MCs connected to the GCD, showing that the network can produce a population gamma rhythm. Connection to the GCD reduces the firing rate and entrains the STOs to a common frequency. The spikes of the MCs do not synchronize (Fig. 1*C Right*); they fire on different cycles of the population rhythm. However, the STOs do approximately synchronize. The amount of synchronization is quantified by the clustering index (CI) and its coefficient of variation (CV) (see *Methods*). Note that the CI for the simulation of MCs with no inhibitory input is >0 (CI = 0.1; CV = 0.54), which is a consequence of the finite time series, with nearby frequencies and finite number of cells. The CI for the system coupled to a single GCD is far greater (CI = 0.73; CV = 0.2). Note that the successive STOs between MC spikes increase their amplitude. The inhibition associated with GCD input partially resets the initial conditions for the STOs (see Fig. S1). Also note that the power of the spiking

Author contributions: J.N.B., L.M.K., and N.J.K. designed research; J.N.B. performed research; J.N.B. and N.J.K. analyzed data; and J.N.B., L.M.K., and N.J.K. wrote the paper.

The authors declare no conflict of interest.

[1]To whom correspondence may be addressed. E-mail: jorgeb@math.bu.edu or nk@bu.edu.

This article contains supporting information online at www.pnas.org/cgi/content/full/0910964106/DCSupplemental.

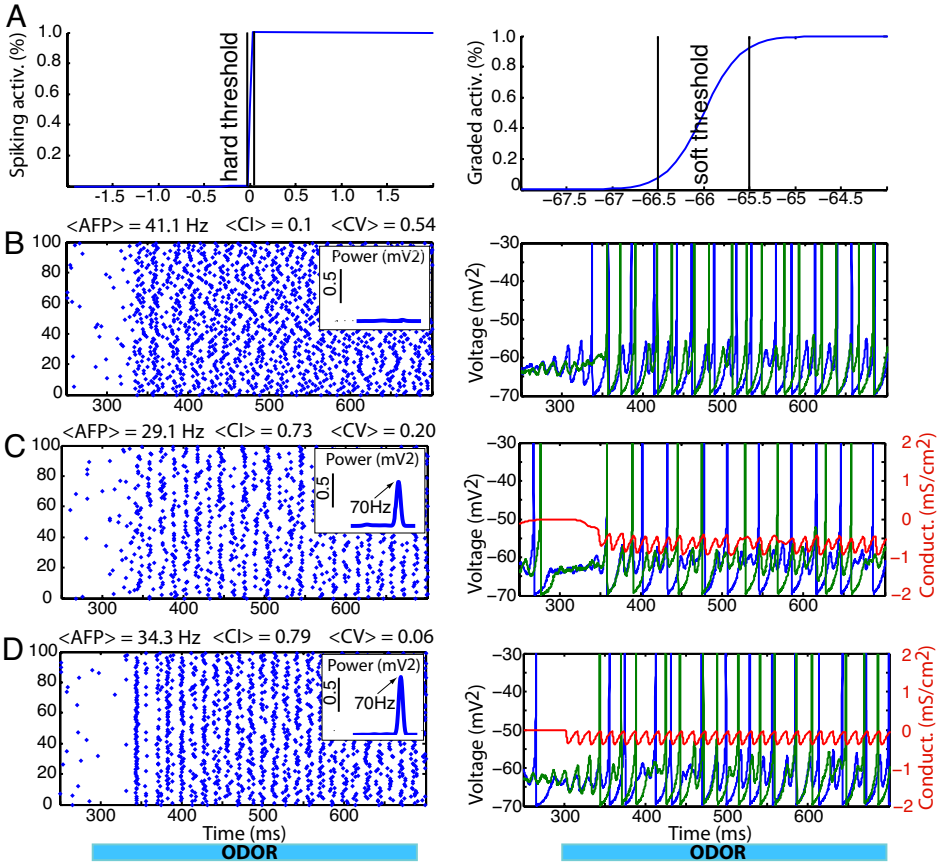


**Fig. 1.** Uncoupled MCs entrained by common inhibitory periodic input. (*A*) Percentage of open channels as a function of voltage for spiking (*Left*) and graded (*Right*) synaptic conductance. (*B–D*) Raster plots of the MC firing (*Left*) showing 450 ms of the 1,600-ms simulation. (*Insets*) The power spectrum, computed during the period of odor stimulation (1,000 ms), for the average MC voltages, which we define as our model spiking local field potential (sLFP). Two random MC voltages vs. time, with the inhibitory conductance overlaid (*C* and *D*), are shown on the right. (*B*) (*Left*) Raster plot for the population of MCs without common inhibition shows no synchronous activity in their firing. Simulated odor is introduced at $t = 300$ ms. The CI of the MC STOs is low but not zero. (*Right*) Voltage activity of two MCs from the population showing their mixed mode behavior of firing with STOs. (*C*) (*Left*) Raster plot for the MCs coupled to a single GCD. The raster plot after odor input becomes more coherent and the CI increases from 0.10 to 0.73. (*Right*) Voltage activity for two MCs are shown with the synaptic conductance from the GCD (red). The frequency of the inhibitory conductance coincides with that of the gamma rhythm of the MC voltage activity. (*D*) Population of MCs entrained by a periodic alpha function inhibitory stimulation. (*Left*) The raster plot shows rhythmic coherent firing of the MCs. (*Right*) Two MC voltages and the periodic input.

model local field potential (sLFP) (see Fig. 1 for definition) in the *Insets* is significantly larger for Fig. 1*C* than for Fig. 1*B*.

The synchronization remains high when the GC is replaced by inhibitory input with a periodic alpha function conductance (Fig. 1*D*). The periodic conductance is modeled on the GCD release of GABA, which occurs during the interval when the GCD voltage is elevated above the threshold for release. In the network, even though the cells receive the same conductance input, they do not receive the same synaptic current, because the postsynaptic voltages are different. Fig. 1*D Right* shows the approximately periodic inhibitory conductance produced by the GCD. Using an alpha function with time constant 3 ms for the conductance yields a comparable pulse of inhibition; the size and shape of the forcing is approximately the same as that produced by the internally generated inhibitory conductance.

When the MC firing rate is low, correlated Gaussian noise input to the MCs does not produce a population gamma rhythm (Fig. S2*A*). Following ref. 11, the Gaussian noise was convolved with an alpha function modeling the effect of synaptic integration. The inhibitory noisy conductance produces sporadic volleys of coherent MC spiking but the sLFP remains incoherent (see Fig. S2*A Inset*). The CI is smaller than in Fig. 1 *C* and *D*, and the high CV shows that the measure is not reliable. If the noise is Poisson distributed with a rate close to that of the STOs ($\lambda$ = Hz) (Fig. S2*B*), the power spectrum is still broad and the CV large. Thus, in our hands, even if the noise itself has a time constant related to that of the STOs, that is not sufficient for good synchronization. For both Gaussian and Poisson noise, the amplitude of the noise was chosen to produce a conductance of similar intensity to that of the $GABA_A$ synapse.

**Synchronization of MC STOs Does Not Require Spikes in the MCs.** Spikes in the MCs are necessary to activate the GCs. However, as shown in Fig. 1*C*, the GCs themselves are not critical to the synchronization if the comparable inhibition is provided. Because the MC spikes are not themselves being synchronized and seem necessary only to produce feedback inhibition, the question arises whether the MC spikes play any role other than for the feedback inhibition in synchronization to the STOs. Fig. 2 addresses that question with a pair of MCs.

We first show in Fig. 2*A* that it is possible to remove the spiking currents of the MCs and retain the STOs. To preserve the approximate amplitude and shape of the STOs we decrease the drive to the MCs compared with Fig. 1, which leads to STOs with amplitudes somewhat larger than those in the full equations for a single MC. Fig. 2*A* shows two uncoupled STOs at ≈70 Hz.

In Fig. 2*B*, we show that the periodic conductance input from Fig. 1*C* also synchronizes the STOs, even if they are detuned; we chose a detuning of >10% in period. With forcing at the same strength and frequency as the inhibition in Fig. 1*C*, the forcing completely synchronizes the STOs. For forcing of half that size, the synchronization is noticeable but not complete (Fig. 2*C*), implying that the current resets that come with MC spiking are not an essential part of the synchronization process. Indeed, the spikes actually make the synchronization more difficult; the same size forcing of the full equations vs. the reduced systems leads to only partial synchronization of the STOs in the former. A significant amount of synchronization persists for the full equations even with 30% detuning (see Fig. S3). In Fig. S1, we show why the STOs are more difficult to synchronize when the MCs spike. The essential reason is that the STOs do not have constant amplitude between spikes and are reset between spikes. Because different MCs spike on different cycles of the population rhythm, the correlated input must synchronize heterogeneous STOs in a small time window (two or three STO cycles).

In Fig. 2*D* we show that the frequency of the STOs can be modulated. To change the STO frequencies, we can either give the

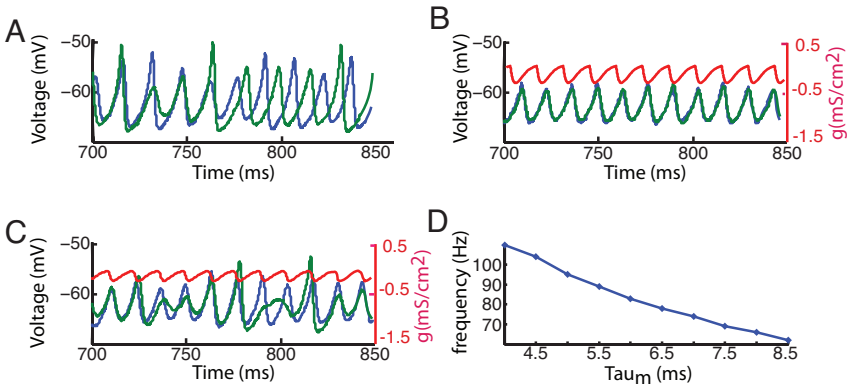


**Fig. 2.** Periodic input can synchronize STOs. (*A*) Spiking currents are not necessary for sustaining the MC STOs. Voltages for two MCs are shown after removing all intrinsic currents except for the $K_s$ and $Na_P$ currents. (*B*) Periodic stimulation (red) strongly synchronizes STOs. The periodic stimulation has the same strength and frequency as in Fig. 1*C* but the synchronization of the STOs in this case is much stronger. (*C*) Decreasing the strength of the stimulation by half still roughly synchronizes the STOs. (*D*) Frequency of STOs depends on the intrinsic properties of the MCs. Increasing the time constant of the activation variable of the slow potassium current decreases the frequency of the STOs.

MCs different drive or change the intrinsic properties of the currents. Changing the values of the drive also changes the STO amplitude significantly. We therefore chose for Fig. 2*D* to change the time constant of the activation variable for the $K_s$ current, which is known to change the frequency of the STOs (6, 12, 13). The STOs depend mainly on the persistent Na and slow K current; thus, the period of the STOs can also be changed by scaling those currents. As discussed in refs. 12 and 13, the interaction of these two currents display resonant behavior to periodic stimulation. In Fig. S4*A* we show that for the parameter values used in this work for $Na_P$ and $K_s$, the resonant frequency is very close to the gamma frequency (≈70 Hz). Decreasing the maximal conductance of both of these currents decreases the value of the resonant frequency (Fig. S4*B*).

**Synchronization of STOs Occurs in a Network with Multiple GCSs and Determines Network Frequency.** In the previous sections, there was one common inhibitory conductance input for all MCs. The same mechanism still works when the network contains 1,000 GCs sparsely and randomly connected to the population of 100 MCs (Fig. 3*A*). Each MC connects reciprocally with 20% of the GCDs. The raster plot (Fig. 3*B*) shows that the population can produce a gamma rhythm, with a subset of the MCs firing on each cycle. As in Fig. 1, the input to the MCs increases from its minimum to maximum value in 50 ms starting at 300 ms. Again, the MC spikes do not synchronize. The GCD voltages are correlated, but not fully synchronized (Fig. 3*C*); thus the MCs are getting partially correlated input.

To show that the population rhythm is that of the STOs, we compare the sLFP power spectrum with the power spectrum of the STOs (called nsLFP for nonspiking LFP). To compute the nsLFP we filter out the spikes (see *Methods*) and calculate the power spectrum of the average of the STOs. Fig. 3*D* shows that they are almost identical in power and peak frequency. We have also performed this simulation with a set of MCs having significantly lower STO frequencies by changing the maximal conductance of the $Na_P$ and $K_s$ currents and the time constant of the activation variable of the $K_s$ current. In that case as well, the population frequency is that of the STO (Fig. S5). Fig. 3*E* shows the power spectrum for the mean field of the GCD voltages; note that it has a gamma peak at the same frequency, but with much less intensity. The CI for the fully connected network is lower than that of the network of MCs with only one GC, but larger than the latter receiving Gaussian or Poisson noise and with a lower CV than for the noisy inputs.

As described in *Methods*, the olfactory receptor neuron (ORN) input consists of Gaussian noise with an increasing mean as the odor is introduced. It can be argued that it is more physiologically realistic to convolve this noise with an alpha function representing synaptic integration. We have not found significant changes in our results when this is taken into account (compare Fig. S6 and Fig. 3*B*).

**Additional Drive to GCDs Changes Power Without (Much) Change in Frequency.** Additional drive to the GCDs mimics added excitatory drive from the piriform cortex and other cortical areas. Increasing drive to the GCDs (from 0.0 to 0.4 $\mu A/cm^2$) decreases the sLFP power, but does not much change the frequency (Fig. 4), which is consistent with the idea that the network frequency is given by that of the STOs, which is not changed by drive to the GCDs. What changes much more when the GCD drive is increased is the average firing rate of the MCs and the CI. The decrease in gamma power with increase in drive is gradual with Fig. 4 showing the two extremes. The increase in GCD drive has the effect of raising the

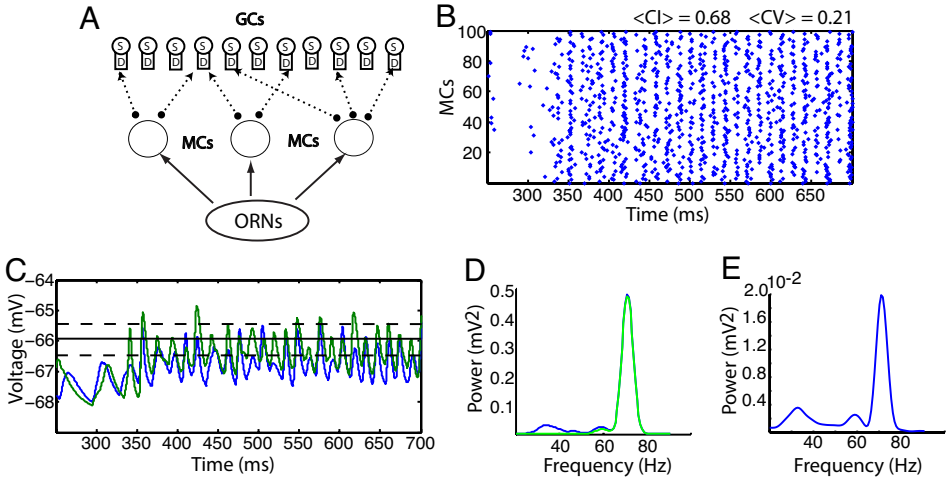


**Fig. 3.** Sparsely connected population of MCs and GCDs can create fast gamma rhythm with frequency determined by the frequency of the STOs. (*A*) Sketch of the dendro-dendritic interaction between 100 MCs and 1,000 GCDs. (*B*) Raster plot showing the spiking activity of the MC population before the odor presentation ($t < 300$ ms) and after odor presentation ($t > 300$ ms). After odor is presented, population frequency (sLFP and snLFP) peaks at 72 Hz. (*C*) Two representative voltage activity traces for the GCDs in the GCD population. The solid line is the half activation value (−66 mV) of the graded synapse, and the dashed lines represent −66 ± 0.2 (see *SI Appendix*). (*D*) Power spectrum for the sLFP (blue) and nsLFP (green) are practically identical. (*E*) Power spectrum for the mean field of the GCD voltage shows that, as a population, the GCD activity oscillates at the same frequency as the MCs (compare with *D*).

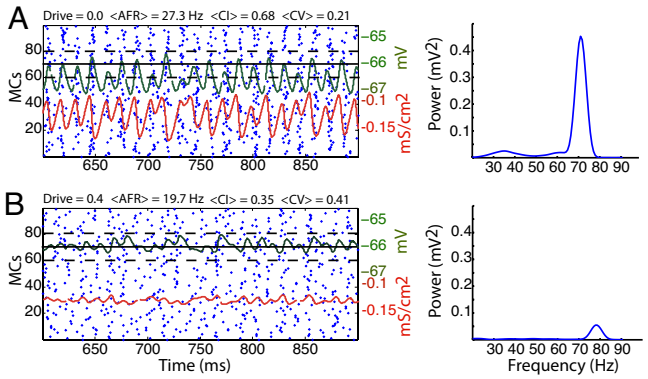


**Fig. 4.** External constant excitatory drive to GCDs decreases power of the sLFP with only a small change in frequency. (*A*) Raster plot (*Left*) and sLFP power (*Right*) show a clear gamma rhythm at (≈70 Hz) for the MC population. The mean field for the GCD subthreshold voltages (green) crosses into and out of the region of graded synaptic activation (black solid and dotted lines). The resultant mean GABAa conductance (red) is also modulated at frequency ≈70 Hz (power spectrum not shown). (*B*) If the GCDs receive too much drive, their voltages remain always above the graded synapse activation threshold and their conductance is almost constant. As a result the MC voltages receive almost constant inhibition incapable of producing a coherent rhythm. This is reflected in the low CI and weak power at the gamma frequency.

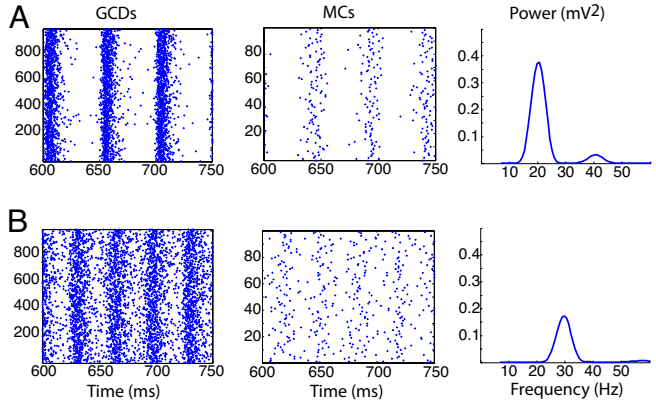


**Fig. 5.** Rhythm frequency depends only mildly on decay time of inhibition. (*A*) Spiking inhibition with decay time 18 ms creates a slow rhythm (≈20 Hz) for the GCD and MC populations, as shown in raster plots (*Left* and *Center*) and power spectrum for the sLFP (*Right*). (*B*) Decreasing the decay time of inhibition 6-fold to 3 ms only increases the rhythm frequency to ≈30 Hz.

GCD voltage to a point where the latter is almost always in the regime corresponding to activation of the graded synapse. Thus, the rhythmicity of the inhibitory input to the MCs is decreased. Therefore centrifugal input can act as a source of desynchronization as observed in refs. 14–16.

**Additional Drive to MCs Changes Spiking Rate, Power, and Frequency.** Additional drive to the MCs mimics increased input from the ORNs. Driving the MCs harder by increasing the mean value of the Gaussian ORN inputs (see *Methods*) increases the spiking rate in the full network, as expected. Less obvious is the effect on sLFP power. The power of the sLFP first increases and then decreases with increased drive (Fig. S7). The differences are associated with changes in the behavior of the GCD population average voltage (as a function of time). As the MCs are driven harder, the GCDs are also driven by the extra firing of the MCs, and their mean voltage over time increases (compare Fig. S7 *A* and *B*). Thus, the graded inhibition is again activated over a larger duty cycle, producing a more uniform conductance forcing. For the largest drive (Fig. S7*C*), the MCs are not coherent. The increase in MC firing shifts the mean GCD voltage permanently above the graded synaptic activation threshold. The frequency of the network increases with drive, but only by ≈10%, as the inhibition also increases with drive to MCs.

It has been shown in experiments that increasing drive to MCs can change the frequency of the STOs (6, 12). There, the MC was isolated, not in a network producing gamma. If we start with a MC whose STO has a frequency of 30 Hz (as in the in vitro work), then increasing the drive to that cell can significantly increase the STO frequency. To produce a MC with STO frequency in the range of 25 to 50 Hz, we revert to the scaling of the $Na_P$ and $K_s$ maximal conductances used in ref. 12. Our results are essentially the same as in ref. 12. Thus, the effect of further drive to a MC can be very different in a single cell than to a cell that is receiving inputs from a population undergoing gamma oscillations.

**Sparse Spiking Inhibition in the GCs Changes the Frequency of Network Rhythm.** So far, all of the inhibition has been graded inhibition. We now replace the graded inhibition by spiking inhibition to see whether that can also produce the gamma rhythm. We also want to make the spiking of the GCDs sparse (10) and keep the spike rate of the MCs lower than the population rate.

We first change the simulation in Fig. 3 by removing the graded inhibition, which also removes some self-inhibition (see *Methods*), allowing the GCDs to spike more readily. Fig. 5*A* shows that this change can lead to a new population rhythm in which the MC spikes are crudely synchronized to produce a population rhythm at a much lower rate. Changing the decay time of inhibition from 18 to 3 ms decreased the period only mildly from ≈50 to ≈33 ms (Fig. 5*B*). If we also double the inhibitory $GABA_A$ maximal conductance (from 0.5 to 1.0 mS/cm$^2$) the frequency remains unchanged (Fig. S8*A*). The resulting rhythm is therefore different from PING, in which the time constant and strength of the inhibition has a large effect on the population frequency.

The lack of tight synchronization of the MCs and GCDs is related to the sparseness of the MC to GCD coupling. If connections are made all–all and the decay time is 3 ms, synchronization at gamma is possible, with the MCs firing at population rate (Fig. S8*B*), which is very much like the PING. The mechanism of this synchronization does not involve STOs (indeed there are no STOs). The all–all connections cause the GCD spikes to fire synchronously, which allows a short effective period of inhibition if the decay time is small enough. In this mechanism, the GCDs fire on every cycle.

Another way to get a gamma population rhythm with GCD spiking is to increase the conductance of the MC to GCD coupling (Fig. S8*C*). In this case, coupling can be sparse, as in Figs. 3 and 5*A*, but the GCDs again fire on almost every cycle. So this parameter range also does not satisfy all of the constraints above. In Fig. S8*D* we show the result of lowering the MC to GCD conductance beyond that of Fig. 5*A* and adding noise to the GCDs to produce sparse GCD spiking; in this case there is almost no power. Thus, in our hands, it was not possible to produce a gamma oscillation with sparsely spiking GCDs while keeping the MC firing rate lower than the population rate.

## Discussion

There is a consensus that dendro–dendritic inhibition plays an important role in synchronization of the MCs (7, 17–19). However, the mechanisms for this synchronization are still controversial: the GCs are known to be able to spike and produce graded inhibition, and the roles of these two types of inhibition in synchronization are unknown. STOs have also been hypothesized to play a role in population oscillations in the OB and elsewhere (6, 13, 20), but it has not been previously shown how such STOs could be synchronized

This article deals with the roles of STOs and different kinds of inhibition (graded and spiking) in the formation of gamma oscil-

lations in the OB. We show that graded inhibition can indeed synchronize MC STOs and keep them synchronized even in the presence of uncorrelated noise and heterogeneity of inputs to MCs. We also show that spiking inhibition can synchronize the STOs, but (in our hands) only when the GCDs spike at high rates comparable to the population rate; reported measurements of spike rates have been much lower (10).

In the model, the time scale for the STOs comes from intrinsic currents of the MCs, notably the slow K current and the persistent Na current. The frequency can be increased (or decreased) by making these currents larger (or smaller); it can also be changed by changes in activation time of the $K_s$ current, or drive to the MCs, as shown in *Results*. Having a range of frequency in the driven STOs is important for the creation of the gamma rhythm when the firing rate is low: it is necessary that some fraction of MCs fire on each cycle to activate the GCs; the noise and the detuning each contribute to the desynchronization of the MC spiking necessary for this. The STO time scale holds the network at a relatively fixed frequency when the GCs are driven harder, as occurs when there is feedback from the piriform cortex, in sharp contrast to the synchronization mechanism of PING, in which stronger excitation of the inhibitory cells leads to a much lower frequency. The ability of the STO frequency to be changed by modulation of intrinsic currents and external drives permits the possibility of different cell assemblies at different frequencies even for comparable drives, which creates a new option for coding of multiple inputs.

The hypothesis that the gamma oscillations do not need GC somatic spikes is supported by ref. 7, which showed that if the GC cell somata are removed, the GCDs, interacting with the MCs, still produce gamma. In a preparation that allows GC spikes, the latter are not significantly locked to the LFP, suggesting these spikes are not a critical part of the process of producing the oscillations. In this article, we consider graded inhibition and dendritic spikes. For the former we use a soft threshold for activation of the inhibitory synapse, with $GABA_A$ release dependent on presynaptic voltage in a graded manner.

Graded inhibition can be mediated by AMPA receptors (AMPARs) in GCDs (21). This release is associated with voltage-gated calcium channels local to GABA release sites, where NMDA receptor (NMDAR)-mediated $Ca^{2+}$ influx can be as much as 1 $\mu$m away from these sites (21–23). Thus, activation of voltage-gated $Ca^{2+}$ channels and subsequent release of GABA can be in proportion to depolarization. One issue is whether the dynamics of the $Ca^{2+}$ channels near the GABA release sites are sufficiently fast to support gamma oscillations. We do not model that here, but leave it as an important problem for future studies. Another issue is whether depolarization of a spine leading to graded GABA release can spread and influence other MCs not synaptically connected to that spine.

The GCDs are known to have both NMDAR and AMPARs,with NMDA being prominent in driving GCD excitation (18). However, it has been shown that, after tetanic stimulation or when GCD excitability is increased or GCD AMPARs have increased decay time constants, the AMPARs are most responsible for GCD excitation (24). We therefore treated the NMDA currents as tonic excitation and did not add this receptor type to the model. There may be several ways of amplifying the excitability of GCDs via neuromodulatory inputs to the external plexiform layer, which may underlie enhancement of gamma oscillations in different cognitive circumstances. A recent study showed that cholinergic drive from M1 receptors on GCDs enhances excitability of GCDs and elevates intracellular $Ca^{2+}$ (19).

The mechanism for synchronization of the MCs by graded inhibition is very different from that of the standard excitation–inhibition interaction that is the basis for the gamma formed by pyramidal cells and proximal fast-spiking interneurons. Unlike the latter, in which the decay time of inhibition is a central parameter (5), in this mechanism the population rhythm is timed by the period of the STOs; changes in drive to the GCs can change the MC firing rate with only small changes in the population frequency. Indeed, the decay time of the inhibition can be changed by 6-fold, with only ≈25% change in period. The uncoupled frequencies of the STOs can be detuned and still have the STOs synchronize, because the GC feedback gives correlated (if not common) input to the collection of MCs. Hence, the system behaves somewhat as if the STOs are independent oscillators with a common forcing, as in classical theory of forced oscillators; the central difference is that the forcing is itself generated by the MC spikes, which activate the GC feedback. However, there is an important difference between the current situation and the classical theory of forced oscillators: as described above and in Fig. S1, when the MCs spike, the STOs are not steady, making STO synchronization harder. The STOs also have to synchronize quickly (before the next spike), in contrast to weakly coupled oscillators (25) that allow synchronization over a large number of cycles. In the limit of very sparse spiking of the MCs, the mechanism is close to that of standard coupled oscillators, but at spiking rates seen experimentally, that limit might not be appropriate. A closer approximation for the MCs might be "resonate and fire" neurons (26), for which there is not yet a theory of synchronization. Such a theory is beyond the scope of this article, but might be facilitated by the work that has been done on mixed-mode oscillations (20, 27–29).

Spiking of the GCs, when it occurs, is believed to be sparse. We asked whether it is possible to produce a gamma rhythm with sparse firing of the GCDs (≈5 Hz) (10). If the inhibition is strictly through spiking synapses, and the connections from MCs to GCDs are sparse, the behavior of the network depends on the maximal conductance of the excitation from the MCs to the GCDs. When the conductance is large enough, it is possible to get a gamma rhythm in which the MCs spike sparsely and the STOs are synchronized. However, in the parameter ranges we tried the GCDs fired on almost every cycle of the gamma rhythm, in contrast to reports from the literature (10). That behavior is similar to persistent gamma produced in neocortex or hippocampus in vitro in the presence of kainate and/or carbachol (4), in which fast spiking interneurons spike at population rates and the pyramidal cells spike at low rates. Reducing the conductance from the MCs to the GCDs also did not produce a gamma rhythm with sparse GCD firing: instead, the population produced a slower rhythm in which the GCDs fired at almost every cycle. This reduction in frequency was related to the spread of the spike times of the GCDs: even with a short inhibitory decay time, the inhibition was sufficiently spread out that it was longer than a STO period in these simulations. The spread of the GCDs is related to the lower conductance of the MC to GCD connection: it requires more MCs to spike to get a GCD to spike, and hence it is not immediately induced after some of the MCs start spiking. If the GCDs are forced to be synchronous (e.g., by using all-all coupling instead of sparse coupling), and the MCs are driven very hard, then there is a gamma rhythm with GCDs again firing on every cycle.

Other models of OB synchronization use different hypotheses. The Bathelier et al. model (12), which produced a gamma rhythm, did not contain physiological GCs; instead, MC spiking led to self and lateral inhibition. Hence, the fictive GCs are essentially spiking on every cycle. The Davison et al. model (30) has detailed biophysical descriptions of both MCs and GCs, with GCDs spiking, but the rhythm produced by that model is, like Fig. 5*A*, lower than the gamma frequency. Schoppa (24) showed experimentally that MCs can be partially synchronized if they get synchronized inhibitory postsynaptic potentials (IPSPs); however, our models suggest that if the MC to GCD connections are sparse and the inhibition is from spiking GCDs, the IPSPs will not be synchronous. In another biophysical model of synchronization of MCs and GCDs, David et al. (31) showed that recurrent inhibition to an initially disorganized MC population could increase the variance of the MC spike timing, suggesting that that sniffing or other early mechanisms of temporal

coordination might be important. However, the gamma oscillations we are describing (32) occur during fast sniffing, when MC spiking is decoupled from sniffing (2). Thus, the situation does not allow a resynchronization with each sniff.

With graded inhibition in our model, correlated noise has a different effect than in that of ref. 11. One major difference in the models is that in ref. 11 the MCs fire at approximately the same rate as the population frequency, ≈25 Hz. In our models the firing rate is approximately the same, but the sLFP frequency is much higher as in ref. 32. With Gaussian or Poisson inputs at the same rate as the firing rate (11) produced synchronization of the MC spikes and therefore the population. In our model, neither produces the synchronization of the STOs (or the population).

In summary, this work proposes a mechanism for the creation of gamma oscillations in the OB, using both STOs in the MCs and graded inhibition from the GCDs. This rhythm differs from both the PING rhythm and persistent gamma in neocortical and hippocampal slices. We also suggest that, with sparse connections and the biophysical properties of GCDs and MCs in the current literature, sparsely spiking GCD synapses (spike rates significantly lower than the sLFP frequency) cannot produce gamma oscillation at the frequencies seen in ref. 32. The model makes predictions about properties of graded inhibition and suggests computational functionality for the OB gamma rhythm.

## Methods

The OB was modeled by using 100 MCs and 1,000 GCs following Hodgkin-Huxley type kinetics. Each MC represents the activity of a single glomerulus; MCs innervating the same glomerulus are assumed synchronous (33). A schematic of the model is shown in Fig. 3*A*. The MCs are single compartment models with fast transient and persistent sodium currents, a delayed rectifier and two transient potassium currents, as described in ref. 12. In ref. 12, the frequency of the STOs was chosen to be in the range of 25 to 50 Hz corresponding to the frequency range observed in vitro (6). We increased the maximal conductances of the $Na_p$ and $K_s$ currents to make the STO frequency 60–90 Hz, as observed in vivo; although this is faster than the STOs seen in vitro, rhythms in vivo are often faster than those in vitro; indeed, the OB gamma is faster in vivo than in vitro (6, 7, 32), and the in vitro gamma is also approximately the same frequency as the in vitro STOs. The periods of the STOs are determined by both intrinsic currents and external drive, and the periods within each simulation are chosen to be over a range of values of ≈10% (see also Fig. S3). In some of the simulations, this detuning comes only from differences in drive, whereas in others there are also differences in intrinsic currents.

Each MC received independent excitatory input from olfactory receptor neurons modeled as a noisy input with rising baseline modeling the introduction of the odor. GCs were modeled with two compartments, a GCD and a GC soma (GCS). The soma was given fast sodium and delayed rectifier potassium currents and M-type and A-type potassium currents. The dendrite was given fast sodium and delayed rectifier currents. Details are from refs. 30 and 34. Because the interaction between the MCs and GCDs is dendro-dendritic, the GCS serves only as a load to the GCD. A more explicit and dynamic role for the GCS becomes evident when other parts of the olfactory system are involved (e.g., the piriform cortex). ORN activity was represented as a noisy Gaussian to the MCs; changes in ORN drive are modeled by changes in mean of Gaussian input (see *SI Appendix* for equations). GCDs were randomly connected to the MCs via reciprocal dendrodendritic synapses with a probability of 0.2.

GCDs receive excitatory input with AMPA kinetics (see *Discussion* for why NMDARs were not considered). In all simulations GABA release can be caused either by spikes (spiking inhibition) or subthreshold depolarization (graded inhibition). For both kinds of synapses the form of the equation for synaptic release is governed by the rise time and decay time. There are differences in the literature about the length of the inhibitory decay time (24, 30). Therefore, we have used decay times of both 18 and 3 ms; there was almost no change in our results. The difference between graded and spiking inhibition is given by the shape of the activation function (sigmoid), whose midpoint sets the activation threshold, and whose slope at that point determines the degree of gradation in dependence of release on voltage (see *SI Appendix*).

To study the coherence of the MC STOs we filtered the spikes from the MC voltage activity. We used the MATLAB function fir1 to band pass filter the signals from 50 to 90 Hz and then used the MATLAB function filtfilt to avoid phase shifts of the signal, which allowed us to approximately preserve the STO structure of the MC voltages while filtering their spikes. To estimate the phase coherence of the MC STOs, we measured the order parameter $C(t)$ as given in *SI Appendix*. The CI was defined as the time average of $C(t)$ during odor stimulation (300–1,300 ms). The CV of $C(t)$ [$CV = \sigma(C(t))/\text{mean}(C(t))$] was also calculated for the same time window corresponding to odor stimulation. The power spectra for the sLFP and snLFP were calculated over one second period during odor stimulation. Each time series is subdivided into three time windows with 50% overlap. All measures were averaged over five trials.

**ACKNOWLEDGMENTS.** We thank P. M. Lledo and B. Ermentrout for helpful suggestions and insights. This work was supported by National Institute on Deafness and Other Communication Disorders Grant R01-DC007995 under the Collaborative Research in Computational Neuroscience program.

1. Balu R, Larimer P, Strowbridge BW (2004) Phasic stimuli evoke precisely timed spikes in intermittently discharging mitral cells. *J Neurophysiol* 92:743–753.
2. Rojas-Líbano D, Kay LM (2008) Olfactory system gamma oscillations: The physiological dissection of a cognitive neural system. *Cognit Neurodyn* 3:179–194.
3. Rinberg D, Koulakov A, Gelperin A (2006) Sparse odor coding in awake behaving mice. *J Neurosci* 26:8857–8865.
4. Whittington MA, Traub RD, Kopell N, Ermentrout B, Buhl EH (2000) Inhibition-based rhythms: Experimental and mathematical observations on network dynamics. *Int J Psychophysiol* 38:315–336.
5. Börgers C, Kopell N (2003) Synchronization in networks of excitatory and inhibitory neurons with sparse, random connectivity. *Neural Comput* 15:509–538.
6. Desmaisons D, Vincent JD, Lledo PM (1999) Control of action potential timing by intrinsic subthreshold oscillations in olfactory bulb output neurons. *J Neurosci* 19:10727–10737.
7. Lagier S, Carleton A, Lledo PM (2004) Interplay between local GABAergic interneurons and relay neurons generates gamma oscillations in the rat olfactory bulb. *J Neurosci* 24:4382–4392.
8. Börgers C, Epstein S, Kopell NJ (2005) Background gamma rhythmicity and attention in cortical local circuits: A computational study. *Proc Natl Acad Sci USA* 102:7002–7007.
9. Börgers C, Epstein S, Kopell NJ (2008) Gamma oscillations mediate stimulus competition and attentional selection in a cortical network model. *Proc Natl Acad Sci USA* 105:18023–18028.
10. Cang J, Isaacson JS (2003) In vivo whole-cell recording of odor-evoked synaptic transmission in the rat olfactory bulb. *J Neurosci* 23:4108–4116.
11. Galan RF, Fourcaud-Trocme N, Ermentrout G, Urban N (2006) Correlation-induced synchronization of oscillations in olfactory bulb neurons. *J Neurosci* 26:3646–3655.
12. Bathellier B, Lagier S, Faure P, Lledo PM (2006) Circuit properties generating gamma oscillations in a network model of the olfactory bulb. *J Neurophysiol* 95:2678–2691.
13. Hutcheon B, Yarom Y (2000). Resonance, oscillation, and the intrinsic frequency preferences of neurons. *Trends Neurosci* 23:216–2222.
14. Gray CM, Skinner JE (1988) Centrifugal regulation of neuronal activity in the olfactory bulb of the waking rabbit as revealed by reversible cryogenic blockade. *Exp Brain Res* 69:378–386.
15. Kay LM, Freeman WJ (1998) Bidirectional processing in the olfactory-limbic axis during olfactory behavior. *Behav Neurosci* 112:541–553.
16. Nusser Z, Kay LM, Laurent G, Homanics GE, Mody I (2001) Disruption of GABA(A) receptors on GABAergic interneurons leads to increased oscillatory power in the olfactory bulb network. *J Neurophysiol* 86:2823–2833.
17. Schoppa NE, Westbrook GL (1999) Regulation of synaptic timing in the olfactory bulb by an A-type potassium current. *Nat Neurosci* 2:1106–1113.
18. Schoppa N, Kinzie J, Sahara Y, Segerson T (1998) Dendrodendritic inhibition in the olfactory bulb is driven by NMDA receptors. *J Neurosci* 18:6790–6802.
19. Balu R, Pressler RT, Strowbridge BW (2007) Multiple modes of synaptic excitation of olfactory bulb granule cells. *J Neurosci* 27:5621–5632.
20. Rotstein HG, Oppermann T, White JA, Kopell NJ (2006) The dynamic structure underlying subthreshold oscillatory activity and the onset of spikes in a model of medial entorhinal cortex stellate cells. *J Comput Neurosci* 21:271–292.
21. Isaacson JS (2001) Mechanisms governing dendritic gamma-aminobutyric acid (GABA) release in the rat olfactory bulb. *Proc Natl Acad Sci USA* 98:337–342.
22. Sassòe-Pognetto M, Ottersen OP (2000) Organization of ionotropic glutamate receptors at dendrodendritic synapses in the rat olfactory bulb. *J Neurosci* 20:2192–2201.
23. Price JL, Powell TP (1970) The synaptology of the granule cells of the olfactory bulb. *J Cell Sci* 7:125–155.
24. Schoppa NE (2006) Synchronization of olfactory bulb mitral cells by precisely timed inhibitory inputs. *Neuron* 49:271–283.
25. Kopell NJ, Ermentrout GB (2002) Mechanisms of phase locking and frequency control in pairs of coupled neural oscillators. *Handbook of Dynamical Systems* (North–Holland, Amsterdam), Vol 2, pp 5–54.
26. Izhikevich EM (2001) Resonate-and-fire neurons. *Neural Networks* 14:883–894.
27. Brons M, Kaper TJ, Rotstein HG (2008) Introduction to focus issue: Mixed mode oscillations: Experiment, computation, and analysis. *Chaos* 18:015101.
28. Yu N, Kuske R, Xian Li Y (2008) Stochastic phase dynamics and noise-induced mixed-mode oscillations in coupled oscillators. *Chaos* 18:015112.
29. Drover J, Rubin J, SU J, Ermentrout B (2004) Analysis of a canard mechanism by which excitatory synaptic coupling can synchronize neurons at low firing frequencies. *SIAM J Appl Math* 65:69–92.
30. Davison AP, Feng J, Brown D (2003) Dendrodendritic inhibition and simulated odor responses in a detailed olfactory bulb network model. *J Neurophysiol* 90:1921–1935.
31. David F, Linster C, Cleland TA (2008) Lateral dendritic shunt inhibition can regularize mitral cell spike patterning. *J Comput Neurosci* 25:25–38.
32. Beshel J, Kopell N, Kay LM (2007) Olfactory bulb gamma oscillations are enhanced with task demands. *J Neurosci* 27:8358–8365.
33. Schoppa NE, Westbrook GL (2001) Glomerulus-specific synchronization of mitral cells in the olfactory bulb. *Neuron* 31:639–651.
34. Bhalla US, Bower JM (1993) Exploring parameter space in detailed single neuron models: Simulations of the mitral and granule cells of the olfactory bulb. *J Neurosci* 69:1948–1965.